BR07 - Experimental Study on Hydrogen Reduction of Bauxite Residue Pellets Using H_2-H_2O Mixtures

Dali Hariswijaya[1], Elias Trondsen Dahl[2], Sivert Ragnhildstveit Erland[3], Jafar Safarian[4]
1. Ph.D. Student
2. Master Student
3. Master Student
4. Professor
Department of Materials Science and Engineering, NTNU,7034 Trondheim, Norway
Corresponding author: dali.hariswijaya@ntnu.no

Abstract

The valorization of bauxite residue through hydrogen reduction followed by magnetic separation of iron and alkaline leaching of non-magnetic part for alumina recovery is a sustainable approach. In this research an experimental study was designed to investigate the effect of temperature and H_2-H_2O gas compositions on the reduction behaviour of iron oxides complex in Bauxite Residue (BR). Green pellets were made from a mixture of bauxite residue and $Ca(OH)_2$ powders, which were subsequently sintered at 1150 °C. The sintered oxide pellets were reduced in a vertical furnace using H_2-H_2O gas mixtures at elevated temperatures using gas compositions ranging from 0-25% H_2O. Total flow of the H_2-H_2O gas mixture was kept at 1 L/min to ensure comparative reduction potentials. X-Ray Diffraction (XRD) and Scanning Electron Microscope (SEM) coupled with energy dispersive spectroscopy (EDS) were employed to characterize the reduced pellets. It was found that the iron oxides exist as complex Brownmillerite phase in the sintered pellets. Lower temperature and higher H_2O content of gas could inhibit reduction of Wüstite to metallic iron. Such behaviour was observed when H_2O gas composition is higher than specific compositions at different temperatures. Pellets reduced at higher temperatures were found to produce significantly smaller pore size but with comparable surface area to pellets reduced at lower temperatures which suggests notably different pore structures.

Keywords: Decarbonisation, Circular economy, Bauxite residue, Hydrogen reduction, Iron.

1. Introduction

1.1 Bayer Process and Bauxite Residue

The Bayer process was invented and patented by Carl Josef Bayer in 1888 and has since then been the leading process for alumina production in the world. The process consists of eight main stages: Milling, desilication, digestion, clarification, precipitation, evaporation, classification, and calcination. In the milling step, the bauxite ore is crushed down into finer particles. Additionally, limestone is added to create a pumpable slurry. After the milling step, the slurry moves through a process called desilication, which involves removing silica (SiO_2). The slurry is then digested using a NaOH solution, which dissolves the aluminum bearing minerals in the bauxite. These minerals include gibbsite ($Al(OH)_3$, boehmite (γ-AlO(OH)) and diaspore (α-AlO(OH)). When the solution is added, the following reactions takes place with gibbsite and boehmite/diaspore, given by Equation (1) and Equation (2**)** respectively [1][2].

$$Al(OH)_{3(s)} + NaOH_{(aq)} \rightarrow Al(OH)^-_{4(aq)} + Na^+_{(aq)} \quad (1)$$

$$AlO(OH)_{(s)} + NaOH_{(aq)} + H_2O_{(l)} \rightarrow Al(OH)^-_{4(aq)} + Na^+_{(aq)} \quad (2)$$

After the processing step, the slurry is cooled down using a series of flash tanks at 1 atm. The slurry is then prepared for clarification where the bauxite residue (BR) is separated away through sedimentation, where chemical additives assist in driving the BR to the bottom of the settling tanks. BR is transferred to washing tanks, where the goal is to recover the caustic soda used in the digestion step. The saturated liquid undergoes a series of filtration steps and BR is left in disposal areas. After clarification, alumina is recovered through crystallization during precipitation step. The precipitation reaction is shown in Equation (3) [1][2].

$$Al(OH)^{-}_{4(aq)} + Na^{+}_{(aq)} \rightarrow Al(OH)_{3(s)} + NaOH_{(aq)} \quad (3)$$

Evaporation of the liquid used during crystallization takes place in heat exchangers, where it is subsequently cooled down afterwards in flash tanks. The condensate that is created through this process is re-used for BR washing or as feed water. Recovered caustic soda is then re-added to the digestion step. The crystals are classified into size ranges, using cyclones and gravity classification tanks. For the coarse crystals, separation from liquid and calcination is performed. For the finer crystals, washing to remove organic impurities and re-addition to the precipitation step is performed. Calcination of the coarse crystals is done by roasting in calciners. The roasting process takes place at temperatures up to 1100 °C. This drives off moisture and water, which eventually creates alumina solids. The calcination reaction is shown in Equation (4) [1][2].

$$2Al(OH)_{3(s)} \rightarrow Al_2O_{3(s)} + 3H_2O_{(g)} \quad (4)$$

1.2 Bauxite Residue Valorization

Red mud, also known as bauxite residue (BR) in dewatered form, is the main by-product generated in the Bayer process. Typically, for each tonne of produced alumina from bauxite ore, about 1.5 tonnes of BR is produced [3]. The generated BR from the Bayer process is stored in large holding ponds, where only 1% to 2% is being recycled [4]. BR typically contains up to 50% of iron oxides. Other compounds found in BR includes silica oxides, titanium oxides, aluminum oxides and other oxides. It is also highly alkaline, with a pH level ranging from 12-13. Due to its high alkalinity, the BR that is stored away in holding ponds poses a great environmental threat to its surroundings. The main way of treating the alkaline BR, is to attempt neutralizing by adding acidic substances, such as HCl [4].

Several studies on BR valorization have been conducted within the past decade which mainly try to recover iron content in BR either in the form of magnetite [5], metallic iron [6] [7][8][9], or clinker [10]. BR reduction with H_2 at low temperature (480 °C) was able to produce magnetite with 87% conversion degree with insignificant metallic iron production [5]. Meanwhile BR reduction with H_2 at high temperature (1000 °C) was able to completely reduce Fe content in BR to metallic Fe [6][7]. However, recovery of Fe-containing phases from solid-state reduced BR remains an issue due to its physical nature which exists in miniscule spots with less than 20 µm in particle diameter [6][7].

Carbothermic reduction of BR beyond Fe melting point (>1538 °C) was able to reliably produce pig iron in its own separated phase [8][9]. The remaining issue was recovery of Al content from its slag where almost half of it was trapped in Gehlenite ($Al_2Ca_2O_7Si$) phase which is difficult to recover via hydrometallurgical means [8]. It is preferred for Al content in slag phase to form highly leachable Mayenite ($Al_{14}Ca_{12}O_{33}$) phase. CaO addition has shown to promote formation of Mayenite phase in reduced BR [8][9]. Another potential valorization of BR is in production of calciumsulfoaluminate-ferrite clinker for specific applications such as adhesive binder [10].

In previous studies there has been a report of discrepancies in thermodynamical data between thermodynamic handbooks and thermodynamic software, such as FactSage, for H_2 reduction of iron oxides such as Wüstite [11]. It is important to remove these discrepancies by verifying them via experimental method. Thus, the aims of the present study were to assess the thermodynamics of reactions between BR and H_2 through comparison of experimental data and thermochemistry calculations and to study the effect of temperature and H_2-H_2O gas compositions on microstructure, morphology, and mineralogy of reacted products.

2. Materials and Methods

An experimental procedure was designed to investigate the effect of H_2-H_2O gas compositions. A mix of BR and $Ca(OH)_2$ was made into sintered pellets and reduced under H_2-H_2O atmosphere. X-ray Diffraction (XRD) and X-ray Fluorescence (XRF) were employed to analyze the sintered pellets. Scanning Electron Microscope (SEM) coupled with energy dispersive spectroscopy (EDS) and XRD were employed to analyze the reduced pellets.

2.1 Pelletizing and Sintering

Table 1. XRF analysis of raw BR, dry basis (normalized, excluding loss of ignition (LOI)).

Composition	Wt%	Composition	Wt%
CaO	9.98	TiO_2	5.67
MgO	0.26	Na_2O	3.51
SiO_2	8.05	K_2O	0.10
Al_2O_3	24.94	P_2O_5	0.13
Fe_2O_3	46.20	SO_3	1.07
MnO	0.09	**Total**	**100**

Table 2. XRF analysis of raw $CaCO_3$ powder, dry basis (normalized, excluding loss of ignition (LOI).

Composition	Wt%	Composition	Wt%
CaO	98.632	TiO_2	0.005
MgO	0.547	Na_2O	0.037
SiO_2	0.208	K_2O	0.035
Al_2O_3	0.175	P_2O_5	0.009
Fe_2O_3	0.084	SO_3	0.263
MnO	0.005	**Total**	**100**

Table 3. XRF analysis of sintered BR pellet.

Composition	Wt%	Composition	Wt%	Composition	Wt%
CaO	29.01	Cr_2O_3	0.18	P_2O_5	0.12
MgO	0.37	V_2O_5	0.15	SO_3	1.03
SiO_2	7.66	TiO_2	3.87	ZrO_2	0.11
Al_2O_3	23.12	NiO	0.06	SrO	0.03
Fe_2O_3	30.52	Na_2O	3.61	Co_3O_4	0.02
MnO	0.04	K_2O	0.10	**Total**	**100**

BR fines were deagglomerated and screened (< 250 μm) to obtain uniform sizing on the mixing process. Raw $CaCO_3$ powder was calcined to make CaO powder. Resulting CaO powder was grinded and screened (< 250 μm) before it was hydrated to make $Ca(OH)_2$ powder. BR fines were mixed with $Ca(OH)_2$ powder and then green pellets were made using a disc pelletizer. Green pellets were screened to obtain pellets with diameter of 4-10 mm which then air-dried for 1 day and subsequently sintered at 1150 °C for 2 hours in exposure to air. The sintered pellets were

cooled down naturally inside the furnace for 8 hours before taken out. Flowsheet of the pelletizing and sintering process is shown in Figure 2, meanwhile XRF analysis of raw BR, $CaCO_3$ powder and sintered pellet are shown in Table 1, Table 2, and Table 3 respectively.

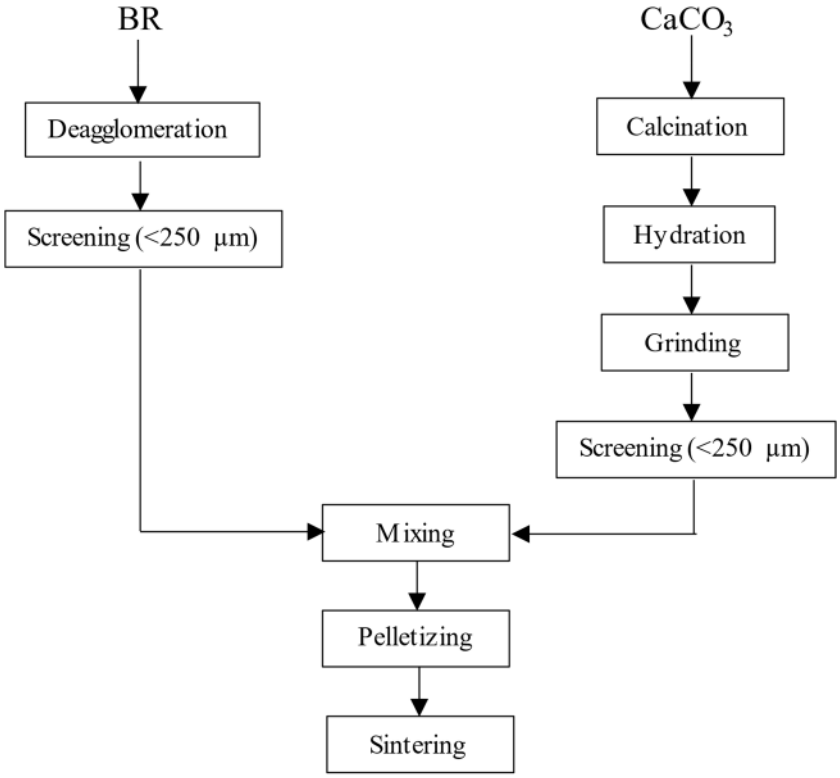

Figure 1. Flowsheet of the pelletizing and sintering process.

2.2 H_2 Reduction

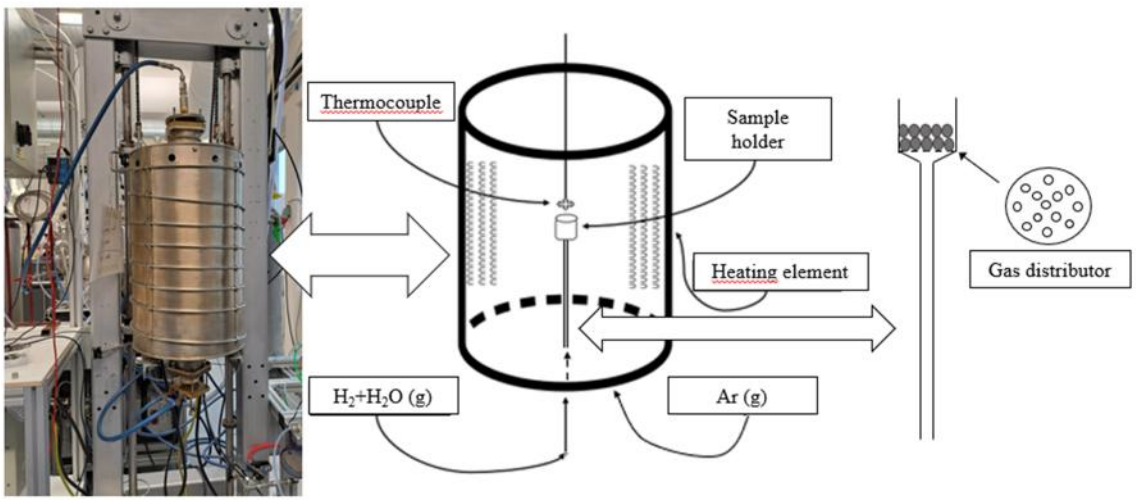

Figure 2. Picture and schematic diagram of reduction furnace.

The reduction experiments were conducted using a vertical alumina tube resistance furnace with an outer metallic alloy heating element. Around 20 grams of sintered pellet was used in every experiment. Shown in Figure 3 is both the furnace and a schematic of its inside. The furnace consists of a cylinder-shaped alumina tube, surrounded by an element that is twined around the furnace. A thermocouple is inserted from the top of the furnace to measure the temperature of the

sample holder. The sample holder is made from Al_2O_3 with gas distributor attached at the bottom to ensure uniform gas distribution to the sample bed. The furnace features a reduction gas inlet positioned at its lower section which goes directly to the sample holder, while the gas, having interacted with the sample, is subsequently leaves through the top gas outlet of the furnace. Another gas inlet at lower section of the furnace which does not go to the sample holder is used to flush the furnace with Ar gas at all times of the experiment to prevent water vapor accumulation in the furnace chamber. The heating and cooling were programmed, while the temperature changes were collected by data logging.

H_2-H_2O gas mix composition was controlled by flowing H_2 gas through a humidifier with set humidity value. The humidifier is P-10 model made by Cellkraft AB which utilizes membrane technology. Experiments were done in 4 different H_2-H_2O gas compositions and 2 different reduction temperatures as shown in Table 4. Heating rate of the furnace was 10 °C/minute and held for 2 hours at set reduction temperature. Total flow of H_2-H_2O gas mix was kept at 1 L/min at all experiments and the furnace was flushed with 1L/min of argon at all times, including the cooling and heating period. Schematic heating diagram of the experiment is shown in Figure 4.

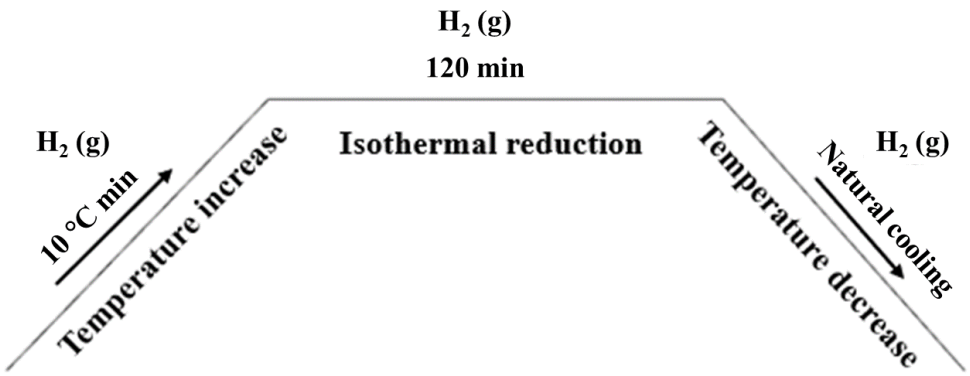

Figure 3. Heating diagram of H_2 reduction experiment.

Table 4. Experiment conditions for H_2 reduction.

No.	Gas composition (vol %)	Reduction temperature (°C)
1	100% H_2 – 0% H_2O	600
2	95% H_2 – 5% H_2O	600
3	85% H_2 – 15% H_2O	600
4	75% H_2 – 25% H_2O	600
5	100% H_2 – 0% H_2O	800
6	95% H_2 – 5% H_2O	800
7	85% H_2 – 15% H_2O	800
8	75% H_2 – 25% H_2O	800

3. Results and Discussion

3.1 Reduction Experiments

Results of the reduction experiments are shown in Table 5. Reduction degree, which was calculated from actual mass losses of the samples, was used to analyze the extent of reduction on every sample. It is assumed that only iron oxides are reduced during the reduction experiment. Formula to calculate the reduction degree is shown in Equation (5).

$$\%W_{red} = \frac{\Delta W_{red}}{W_{O,Fe_2O_3}} \cdot 100\% \quad (5)$$

where:

$\%W_{red}$ Reduction degree
ΔW_{red} Mass loss during the experiments, kg
W_{O,Fe_2O_3} Total mass of oxygen in Hematite, kg

Reduction experiments showed that reduction of iron oxides in the sample requires significantly higher H_2/H_2O ratio compared to the value showed in the Ellingham diagram [12]. The difference in H_2/H_2O equilibrium value is due to the difference in the activity of iron oxides, since in the Ellingham diagram the oxides are pure with chemical activity as unity. Previous study has also shown that iron in sintered BR pellets mainly exists as calcium ferrite in complex phases such as Brownmillerite ($Ca_2[Al,Fe]_2O_5$) and Srebrodolskite ($Ca_2Fe_2O_5$) [13].

Table 5. Mass changes in reduction experiments and the calculated reduction degrees.

No.	Gas composition (vol %)	H_2/H_2O	T (°C)	Initial mass (g)	Mass loss (g)	Reduction degree (%)	Lowest oxidated state
1	100% H_2 – 0% H_2O	∞	600	20.0801	0.9473	49.64	Metallic Fe
2	95% H_2 – 5% H_2O	19	600	20.0191	0.4862	25.56	Metallic Fe
3	85% H_2 – 15% H_2O	5.7	600	20.0764	0.3476	18.22	Wüstite
4	75% H_2 – 25% H_2O	3	600	20.0273	0.2985	15.68	Wüstite
5	100% H_2 – 0% H_2O	∞	800	20.0664	1.3779	72.26	Metallic Fe
6	95% H_2 – 5% H_2O	19	800	20.0073	1.3661	71.85	Metallic Fe
7	85% H_2 – 15% H_2O	5.7	800	20.0757	1.325	69.45	Metallic Fe
8	75% H_2 – 25% H_2O	3	800	20.1392	0.4249	22.20	Wüstite

It was observed from the experiments that metallic Fe reduction at 600 °C and 800 °C was achieved starting from H_2/H_2O = 19 and H_2/H_2O = 5.7 respectively. Furthermore, H_2 reductions at 600 °C showed significantly slower kinetic compared to reductions at 800 °C, which was indicated by presence of metallic iron in one of the reduced samples but with much lower reduction degree. During 600 °C reduction experiments metallic iron was found starting from H_2/H_2O ratio of 19, but in a small amount and alongside presence of Wüstite. This can be caused by either slow reaction kinetics or reduction condition that is very close to the actual equilibrium value. On another note, the absence of Wüstite in sample reduced at 800 °C with H_2/H_2O ratio of 5.7 suggests that the actual equilibrium value is significantly lower than 5.7.

To verify the results, theoretical equilibrium conditions was calculated based on thermodynamical software database and established thermochemistry data compiled by Turkdogan [14]. FactSage and HSC was used to obtain value of Fe_2O_3 activity in $Ca_2Fe_2O_5$ and equilibrium constant respectively. The resulting calculated equilibrium H_2/H_2O ratio from each source of database was compared to the values from experimental results as shown in Table 6. Reaction which are used to calculate equilibrium constant in HSC is shown in equation (6).

$$\frac{1}{3}Fe_2O_3 + H_2 = \frac{2}{3}Fe + H_2O; \quad K = \frac{p_{H_2O} \cdot {a_{Fe}}^{2/3}}{p_{H_2} \cdot {a_{Fe_2O_3}}^{1/3}} \quad (6)$$

where:

K Equilibrium constant
p_{H_2O} Partial pressure of water vapour
p_{H_2} Partial pressure of hydrogen
a_{Fe} Activity of metallic Fe
$a_{Fe_2O_3}$ Activity of Fe_2O_3

Calculated theoretical values of equilibrium conditions from thermodynamical database and Turkdogan's thermochemistry data shows similar values of H_2/H_2O ratio within the expected uncertainties. Observed experimental results on every reduction temperature and H_2/H_2O ratio were in agreement with calculated values as well. However, the experimental conditions which produces nearest condition to theoretical equilibrium for each temperature are done at higher H_2/H_2O ratio than calculated equilibrium value to some extent. Thus, more experiments need to be done with smaller steps of H_2/H_2O ratio to accurately predict the actual equilibrium condition.

Table 6. Calculated and observed values of H_2/H_2O ratio for Fe reduction in $Ca_2Fe_2O_5$.

T (°C)	$a_{Fe_2O_3}$ (Factsage)	K (HSC)	K (Turkdogan)	Calc. H_2/H_2O (HSC)	Calc. H_2/H_2O (Turkdogan)	Obs. H_2/H_2O
500	1.88×10^{-4}	0.87	0.68	20.03	25.68	No data
600	3.70×10^{-4}	1.34	1.04	**10.38**	**13.38**	**≈19**
700	6.66×10^{-4}	1.85	1.46	6.20	7.84	No data
800	1.11×10^{-3}	2.37	1.92	**4.07**	**5.02**	**<5.7**
900	1.69×10^{-3}	2.91	2.42	2.88	3.48	No data
1000	2.43×10^{-3}	3.46	2.93	2.15	2.54	No data

3.2 XRD Analysis

XRD analysis on sintered pellets showed that initial major compounds in the pellets were Brownmillerite, Mayenite, Gehlenite, Hematite and Titanite ($CaSi[Ti,Al]O_5$) as shown in Figure 4.

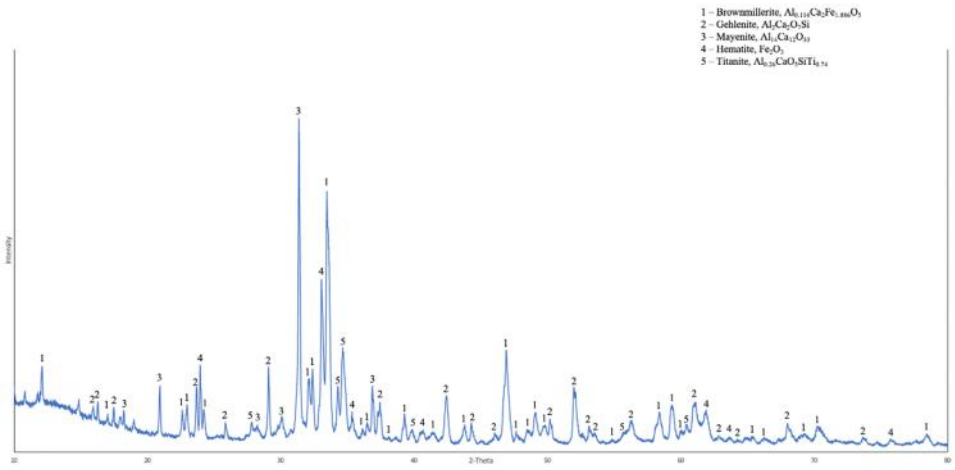

Figure 4. XRD analysis of sintered BR pellet.

XRD results of pellets reduced at 600 °C confirmed that metallic Fe starts to appear at H_2/H_2O = 19 and higher as shown in Figure 5. Srebrodolskite peaks were detected instead of Brownmillerite in XRD spectra of reduced pellets, however since both of them have similar peak characteristics Srebrodolskite peaks were treated as Brownmillerite in the analysis. Metallic Fe peaks were observed to increase with higher H_2/H_2O ratio meanwhile Gehlenite, Brownmillerite and Perovskite peaks were relatively unchanged. This suggests that reduction of iron oxides in the Brownmillerite complex happened without breaking down the Brownmillerite complex itself and none of the other oxides in the sample were reduced during the experiment which confirmed the assumption for calculation of reduction degree in the reduced samples.

XRD results of pellets reduced at 800 °C, as shown on Figure 6, confirmed previous trends where Fe peaks was observed to increase with increasing H_2/H_2O ratio meanwhile Gehlenite,

Brownmillerite and Perovskite peaks were relatively unchanged. Metallic Fe peaks start to appear at H_2/H_2O = 5.7 which is significantly lower compared to pellets reduced at 600 °C. Furthermore, all of the Magnetite peaks were gone starting from at H_2/H_2O = 5.7 which suggests that actual value of H_2/H_2O ratio at the equilibrium of FeO reduction into metallic Fe is significantly lower than 5.7. Another important highlight from Figure 6 is the emergence of Mayenite peaks which were absent on Figure 5. Previous studies showed that H_2 reduction of BR produced Mayenite as one of its end products which has higher recovery potential for its alumina content through hydrometallurgical process compared to Gehlenite [7][15]. Furthermore, amount of Mayenite phase in reduced BR was shown to be strongly related to reduction temperature [7]. Based on those studies it is suggested that the absence of Mayenite peaks on pellets reduced at 600 °C is due to lower reduction temperature. Thus, H_2 reduction process of BR should be done at T > 1000 °C to allow effective recovery of alumina in BR.

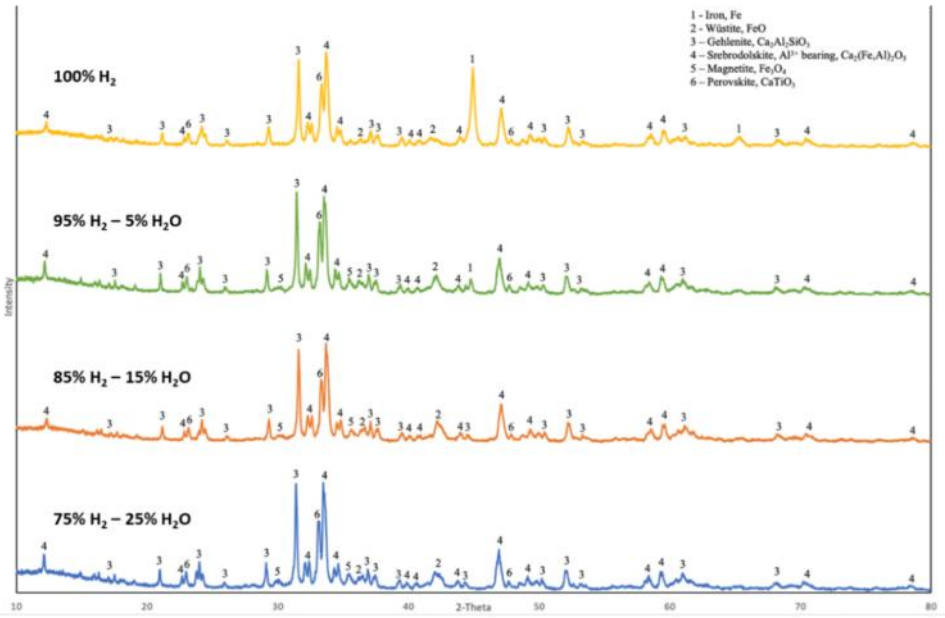

Figure 5. XRD analysis of BR pellets reduced at 600 °C.

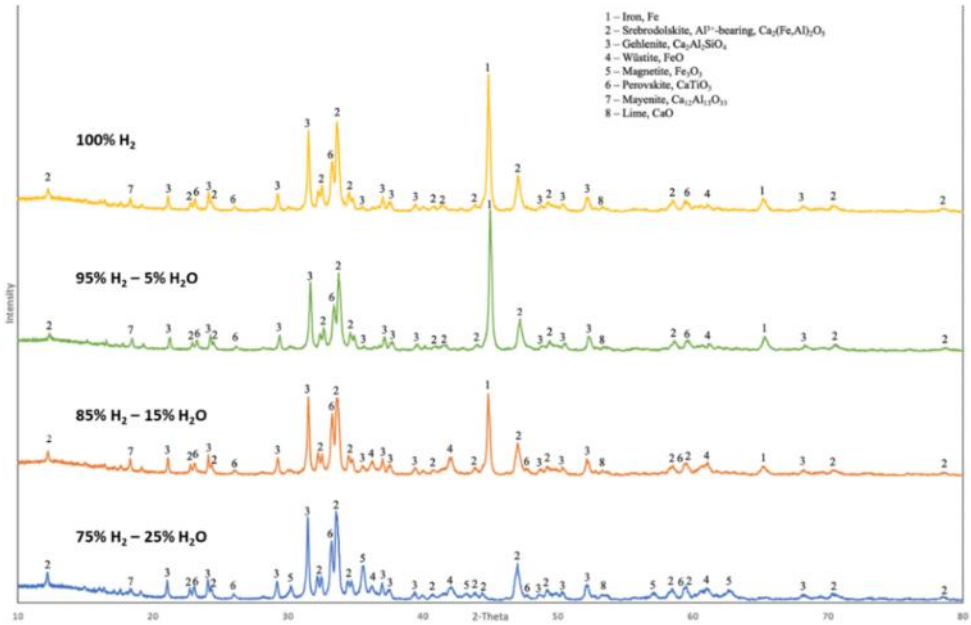

Figure 6. XRD analysis of BR pellets reduced at 800 °C.

3.3 SEM Analysis

SEM analysis of the samples reduced at 600 °C and 800 °C is shown on Figure 7 and Figure 8, respectively. SEM images suggested that partial sintering starts to occur at 800 °C which significantly lowers average pore size of the reduced pellets while retaining similar surface area due to high degree of reduction and the corresponding pore evolution.

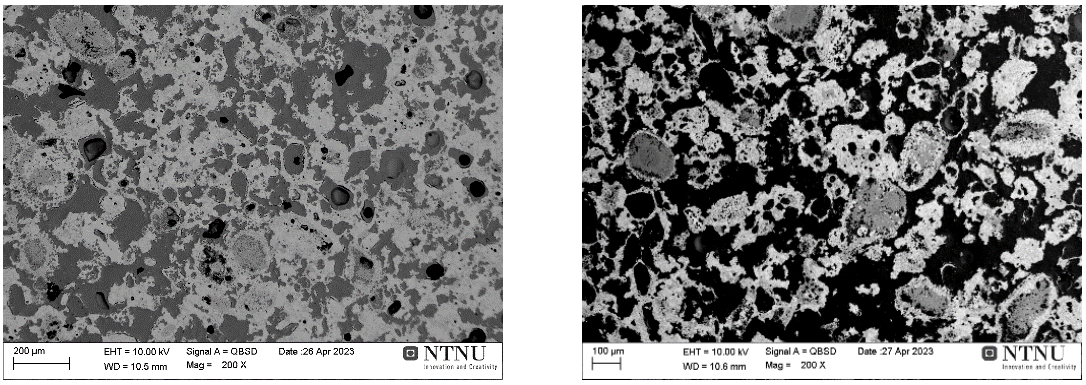

Figure 7. SEM images of pellets reduced at 600 °C with different reduction atmosphere. Left: 75% H_2 – 25%H_2O, right: 100% H_2.

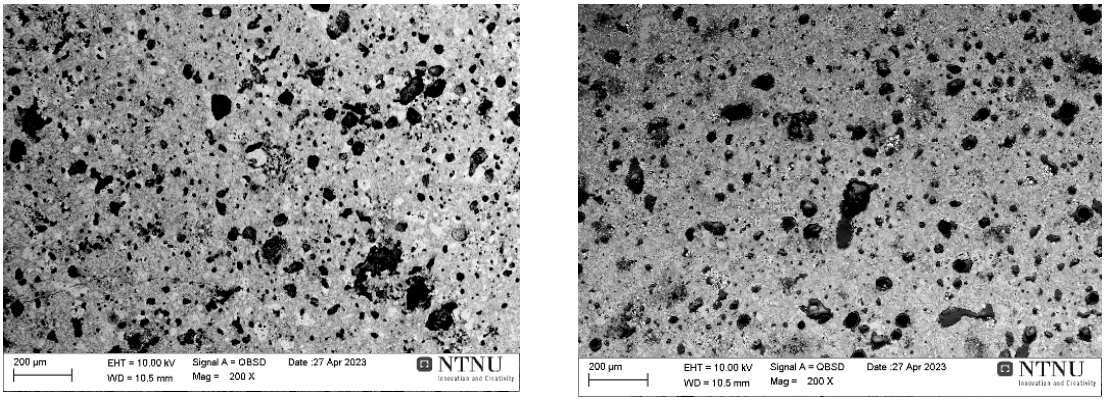

Figure 8. SEM images of pellets reduced at 800 °C with different reduction atmosphere. Left: 75% H_2 – 25% H_2O, right: 100% H_2.

From the calculated values of reduction degree, it can be concluded that higher H_2/H_2O ratio leads to higher extent of iron reduction in the sample. Higher reduction extent generally means higher amount of oxygen atoms removed from the sample, producing pores and cracks in the reduced sample and enlarging existing pores. However, this behaviour was only observed on samples reduced at 600 °C. As shown in Figure 7, samples reduced at 600 °C with 100% H_2 gas composition has significantly larger pore amount and volume compared to sample reduced with 75% H_2 – 25% H_2O gas composition. Meanwhile, as shown in Figure 8, for samples reduced at 800 °C there was no significant difference between pore structure of the sample reduced with 100% H_2 gas composition and the one reduced with 75% H_2 – 25% H_2O gas composition. This suggests that the whole pore structure in the sample was completely reformed due to partial sintering in the sample, producing similar pore structure in all samples reduced at 800 °C. It is expected that at higher temperatures (T > 800 °C) sintering mechanism will have an even more dominant role in pore evolution of H_2 reduced BR pellets compared to pore enlargement and creation due to oxygen atoms leaving the pellet.

4. Conclusions

- Equilibrium condition for H_2 reduction of metallic Fe at 600 °C was observed at $H_2/H_2O \approx 19$ meanwhile at 800 °C it was observed at $H_2/H_2O \leq 5.7$.
- Iron oxides were the only oxides reduced during the reduction process in the experiments, all the other metal oxides were not reduced as confirmed by XRD analyses.
- Iron in sintered BR pellets exists largely as calcium ferrite in form of a Brownmillerite complex as confirmed by XRD and equilibrium calculation using thermodynamical software and database.
- Obtained experimental results are in accordance with calculated equilibrium conditions.
- More experiments with smaller steps of H_2/H_2O ratio need to be done to obtain more accurate figures on actual equilibrium condition.
- Sintering mechanism plays a major role in pore development during reduction process, higher reduction temperature causes more sintering and porosity loss.

5. References

1. R. E. Smallman, R. J. Bishop, "Chapter 10 – Ceramics and Glasses", *Modern Physical Metallurgy and Materials Engineering*, 6th Edition, Butterworth-Heinemann, 1999, 320-350.
2. Refining Process, *World Aluminum*, https://bauxite.world-aluminium.org/refining/process/ (Accessed on 20 May 2023).
3. A. K. Pandey, R. Prakash, Opportunities for Sustainability Improvement in Aluminum Industry, *Engineering Reports*, 2020, e12160. https://doi.org/10.1002/eng2.12160
4. C. Brunori et al., Reuse of a Treated Red Mud Bauxite Waste: Studies on Environmental Compatibility, *J. Hazard. Mater.*, vol.117, no. 1, (2005), 55-63.
5. M. Samouhos et al., Controlled Reduction of Red Mud by H_2 followed by Magnetic Separation, *Minerals Engineering*, 2017, 105, 36-43.
6. M. K. Kar, C. van der Eijk, and J. Safarian, Hydrogen Reduction of High Temperature Sintered and Self-Hardened Pellets of Bauxite Residue produced via the Addition of Limestone and Quicklime, *Proceedings of 40ht International Conference of ICSOBA*, 10-14 October 2022, Athens, Greece, *TRAVAUX* 51, 823-833.
7. O. B. Skibelid et al., Isothermal Hydrogen Reduction of a Lime-Added Bauxite Residue Agglomerate at Elevated Temperatures for Iron and Alumina Recovery, *Materials*, 2022, 15, 6012. https://doi.org/10.3390/ma15176012 (Accessed on 20 May 2023).
8. Adamantia Lazou et al., The Utilization of Bauxite Residue with a Calcite-Rich Bauxite Ore in the Pedersen Process for Iron and Alumina Extraction, *Metallurgical and Material Transactions B*, 2021, 52B, 1265.
9. K. E. Ekstroem et al., Recovery of Iron and Aluminum from Bauxite Residue by Carbothermic Reduction and Slag Leaching, *Journal of Sustainable Metallurgy*, 2021, 7, 1314-1326.
10. Tobias Hertel et al., Boosting the use of Bauxite Residue (Red Mud) in Cement – Production of an Fe-rich Calciumsulfoaluminate-ferrite Clinker and Characterisation of the Hydration, *Cement and Concrete Research*, 2021, 145, 106463.
11. Shuyue Chen et al., Themodynamic Study of H_2-FeO Based on the Principle of Minimum Gibbs Free Energy, *Metals*, 2023, 13, 225.
12. P. Atkins, J. de Paula, *Physical Chemistry: Thermodynamics and Kinetics*, 8th Edition, W.H. Freeman, 2006.
13. Manish Kumar Kar and Jafar Safarian, Characteristics of Bauxite Residue-Limestone Pellets as Feedstock for Fe and Al_2O_3 recovery, *Processes*, 2023, 11, 137.

14. E. T. Turkdogan, *Physical Chemistry of High Temperature Technology*, New York, Academic Press, 1980, 10-25.
15. M. K. Kar, C. van der Eijk, and J. Safarian, Kinetics Study on the Hydrogen Reduction of Bauxite Residue-Calcite Sintered Pellets at Elevated Temperature, *Metals*, 2023, 13, 644. https://doi.org/10.3390/met13040644.